

# Fast Recovery Studies on Thermal Window based Dielectric for HTS Cable

Harris K. Hassan\* and Abhay Singh Gour

Cryogenic Engineering Centre, Indian Institute of Technology, Kharagpur – 721302, West Bengal, India; harriskhassan@gmail.com

## Abstract

High Temperature Superconducting (HTS) cables have remarkable electric power transmission characteristics compared to conventional power cables. Thus, HTS cables are suitable for the sustainable electrical grids of the future. Electric faults of various origins and durations are inevitable in a commercial electric power transmission network. The integration of HTS cables to these networks requires reliable cable operation under fault conditions. However, it was found that HTS cables require a long recovery interval after the fault and subsequent quench. It is primarily attributed to the high thermal resistance of the cable dielectric layer. An innovative dielectric design is proposed in this article to improve the thermal performance of HTS cables and the results are compared with that of a conventional HTS cable. Transient thermal analysis was carried out to determine the recovery interval and the electric insulation characteristics were studied using an electrostatic analysis. Both studies were performed using Finite Element Analysis (FEA). It was found that a reduction in the recovery interval is possible without deterioration in the electric insulation level.

**Keywords:** Finite Element Analysis, Quench in HTS Cables, Recovery Interval, Thermal Window based Dielectric

## 1. Introduction

High Temperature Superconducting (HTS) power transmission cables with their various advantages are capable of replacing the existing power transmission lines. Since the electric faults associated with the commercial power transmission network are inevitable, the reliability of HTS cable designs during these extreme operating conditions should be evaluated<sup>1</sup>. Electric faults of various origins and durations may happen and they all result in abnormal amount of voltage and current in the transmission lines<sup>2</sup>. Even with sophisticated protection systems, the fault current may pass through the conductor for a limited period. Besides, the large power transmission capacity, critical operating environment and the high electrical resistivity of HTS material at the normal state make the consequences of fault in HTS cables severe relative to the conventional cables<sup>3</sup>.

### 1.1 Structure of a Cold Dielectric (CD) HTS Cable

Various parameters govern the design of HTS cables which resulted in different cable configurations. A

principal division is based on the type of dielectric used. A Warm Dielectric (WD) HTS cable has its dielectric layer wound outside the cable cryostat at the ambient temperature. Contrastingly, the Cold Dielectric (CD) HTS cable contains the dielectric layer inside the cable cryostat immersed in the cryogen. Even though the CD HTS cables are expensive and difficult to manufacture, they are preferred over WD HTS cables due to their high efficiency, less maintenance and ease to retrofit to the present infrastructure<sup>4</sup>.

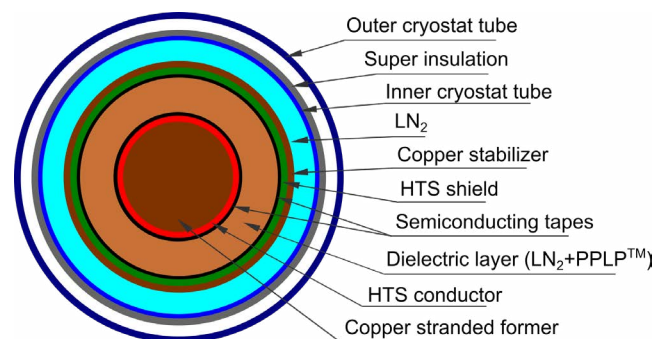


Figure 1. Cross-section of a single phase CD HTS cable.

The cross-section of a Cold Dielectric (CD) HTS cable is shown in Figure 1. The required number of HTS tapes for the rated power transmission is helically wound on a former made of stranded copper wire. This serves as an initial bypass for the transport current if the magnitude exceeds the critical current of the HTS tapes. A layer of semiconducting tapes is wound over the HTS tapes before the dielectric layer to smoothen out the high electric field gradient<sup>5</sup>. The dielectric layer is designed according to the voltage level of the cable. A liquid nitrogen impregnated PPLP™ (composite) dielectric is commonly used in HTS cables. It consists of butt gaps filled with liquid nitrogen (LN<sub>2</sub>) between consecutive turns of PPLP™. Another layer of semiconducting tape is wound over the composite dielectric layer. The outer shield layer consists of HTS tapes and their copper stabilizers. It serves the purpose of shielding the magnetic field from the cable core<sup>6</sup>. This concentric multilayered structure with its protective layer is known as the core of HTS cables. The HTS cable core is housed inside a LN<sub>2</sub> cryostat using spacers to keep the cable aligned axially. The double-layered cryostat is fabricated using corrugated steel tubes. LN<sub>2</sub> flows in the annular space between the cable core and the inner cryostat wall. Heat transfer from the ambient to the LN<sub>2</sub> is limited by using super insulation between the inner and outer cryostat walls.

## 1.2 Electric Fault in CD HTS Cables

During the fault in HTS cables, the magnitude of transport current exceeds the critical current of HTS tapes leading to the loss of superconductivity. This phenomenon is known as quench. The electrical resistivity value of a quenched superconductor is several orders of magnitude larger than that of copper<sup>7</sup>. Since the cable former and the HTS layer are electrically connected, the fault current will be initially shared and later flows entirely through the copper former until the protection system isolates the cable from the grid. Even though the duration of current flow is in the order of milliseconds, the immense magnitude of fault current,  $I_{\text{fault}}$  through a resistive medium is enough to generate an extreme amount of thermal energy<sup>1,3</sup>. This results in an instantaneous increment of HTS layer temperature until the fault current disappears<sup>8</sup>.

The generated heat,  $Q_{\text{gen}}$  at the centre of the cable travels in the radial direction through multiple layers of the cable towards LN<sub>2</sub> at the annular region as shown in Figure 2. When the heat reaches the butt gaps in the

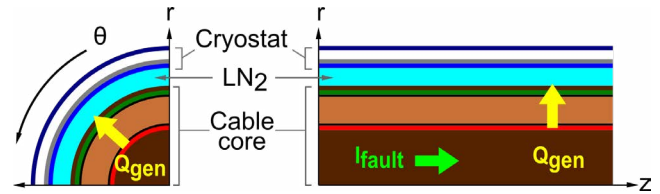


**Figure 2.** Heat transfer in a quenched CD HTS cable.

composite insulation, LN<sub>2</sub> evaporates creating bubbles locally<sup>9</sup>. Consequently, partial discharge can happen and the insulation resistance level reduces. Besides, the low thermal conductivity of gaseous nitrogen reduces the heat transfer efficiency of the composite insulation. Since the heat generated has to be carried away by the LN<sub>2</sub>, the temperature of the cryogen also increases. Multiple faults cause thermal cycling of HTS tapes which in turn degrade their power carrying capacity or even result in the burnout of the cable<sup>1</sup>.

After the fault, immediate re-entry of the operating current through the quenched HTS cable is not possible. It requires a certain amount of time to dissipate the heat so that the cable temperature reduces to the operating temperature of the cable. This period is known as the recovery interval or recovery time<sup>9</sup>. It was found that the cable recovers only when the warm cryogen in the annular flow channel is replaced by the cold cryogen. However, the recovery interval of CD HTS cables is long and it ranges from 300 s to 8 hours depending on the HTS cable design<sup>3,10</sup>. Thus, HTS cables cannot operate immediately after a fault induced quench which limits their commercial application.

It can be seen from Figure 2 that the dielectric layer occupies the largest volume between the former and the cryogen flowing in the annular region. Heat is generated rapidly at the cable former. However, the low thermal conductivity of PPLP™ ( $\kappa_{\text{PPLP}}^{\text{TM}} = 0.05 \text{ W/m-K}$  at 77 K) which constitutes the dielectric layer acts as a thermal barrier. Hence, the Joule heating at the former can be considered as quasi-adiabatic which results in a steep temperature rise of the HTS conductor layer. Later, the accumulated thermal energy is dissipated very slowly through the dielectric layer to LN<sub>2</sub><sup>1,3,8,11</sup>. Furthermore, the delayed heat transfer causes heating of LN<sub>2</sub> even after the duration of fault causing a slow recovery of the cable<sup>9</sup>.

## 1.3 Dielectric Layer with Thermal Windows

Presently, the problem is partially solved by increasing the cable former diameter and thereby reducing the Joule

heat<sup>1,3</sup>. However, this results in unwanted thermal load, large size, weight and reduced flexibility of the cable. It is possible to solve the low thermal performance of the dielectric layer by replacing PPLP<sup>TM</sup> with dielectric materials of high thermal conductivity. However, their use cannot be justified with the low benefit-to-cost ratio considering the long length of power transmission lines. Hence, a cost-effective method to enhance the thermal characteristics of the dielectric layer of HTS cables is required. Nevertheless, the electrical insulation resistance level required for the cable has to be ensured.

This article introduces a solution to the above-stated problems by improving the thermal characteristics of the HTS cable dielectric layer without compromising on its electrical insulation resistance level. During the fabrication of HTS cables, the dielectric material with better thermal characteristics can be wound intermittently with PPLP<sup>TM</sup> tapes. This will provide paths of low thermal resistance and they are called as ‘thermal windows’ between the former and the cryogen as shown in Figure 3. The heat generated during the quench transfers rapidly through these channels from the cable core to the LN<sub>2</sub>. For the present study, Kapton constitutes thermal windows while the rest of the dielectric layer is composed of PPLP<sup>TM</sup> and LN<sub>2</sub>. Since the thermal characteristics of Kapton are superior to that of PPLP<sup>TM</sup> as given in Table 1, an enhanced heat transfer between the cable core and cryogen in the annular flow path can be observed. However, it has to be ensured that the introduction of thermal windows to the dielectric layer may not hamper its primary function of confining the electrical fields emitting from the high voltage conductor.

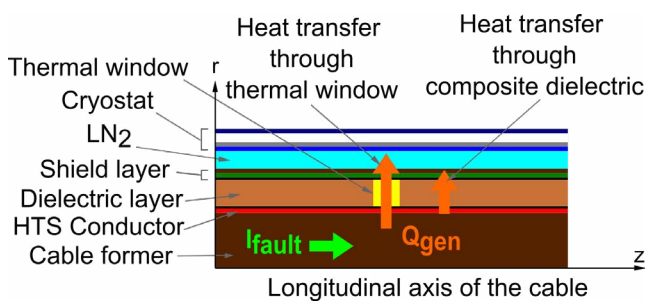


**Figure 3.** Longitudinal section of CD HTS cable having thermal windows in the dielectric layer.

The composite dielectric used in HTS cables consists of butt gaps filled with LN<sub>2</sub>. Their dimensions and distribution depend upon the PPLP<sup>TM</sup> tape and its winding parameters. In the resulting dielectric configuration, LN<sub>2</sub>

inside the butt gaps will be surrounded by PPLP<sup>TM</sup>. The relative permittivity of LN<sub>2</sub> is less than that of the PPLP<sup>TM</sup> by approximately 60% as given in Table 2. Consequently, the electrical stress concentration occurs and may result in partial discharge at voltage levels lower than the electrical breakdown strength of PPLP<sup>TM</sup><sup>12</sup>. Thus, the proposed dielectric design can be considered safe only if the electrical stress due to the thermal window does not exceed the electrical stress inside the composite dielectric.

**Table 1.** Thermal properties of Copper – OFHC, PPLP<sup>TM</sup> and Kapton at 73 K<sup>13-16</sup>.

Property	Copper OFHC	PPLP <sup>TM</sup>	Kapton
Density, $\rho$ (kg / m <sup>3</sup> )	9080	1098	1420
Thermal conductivity, $\kappa$ ( W / m-K )	520	0.05	0.4
Specific heat capacity, $C_p$ ( J / kg-K )	193.4	430	359.154

The objective of the study is to investigate the thermal performance of HTS cables with the dielectric layer having thermal windows after a quench induced by fault. The specifications of the HTS cable selected for the analysis are given in section 2. Transient thermal analysis of the HTS cable was conducted using Finite Element Analysis (FEA) to determine its thermal recovery interval. Furthermore, an electrostatic simulation was performed to analyze the electric field distribution inside the composite dielectric layer with thermal windows. The numerical solution methodologies used in FEA for both thermal and electrostatic studies are described in section 3. The results were compared with that of HTS cables having a conventional dielectric layer in section 4. Finally, the findings are concluded in section 5.

**Table 2.** Relative permittivity of PPLP<sup>TM</sup>, LN<sub>2</sub> and Kapton at 73 K and 1 kHz<sup>17-19</sup>

Material	Relative permittivity, $\epsilon_r$
PPLP <sup>TM</sup>	3.71
LN <sub>2</sub>	1.42
Kapton	3.25

## 2. HTS Cable Specifications

Numerous superconducting cable demonstration projects can be found in the literature at various stages

of completion<sup>20</sup>. Among them, the Albany, NY HTS Cable Project is remarkable with its 7000 hours of in-grid operation. The details of the project including its design, assembly, testing and installation are presented in various articles<sup>6,21,22</sup>. Since reliable fault current test results are available for this project; the present study uses these values to numerically analyze the fault and the following thermal behaviour of the cable.

## 2.1 HTS Cable Model and Fault Characteristics

The important parameters of the HTS cable used for the present investigation are given in Table 3. In a 3-in-One (Triad) type HTS cable, each phase has a dedicated cable core as illustrated in Figure 4. Thus, three cable cores are contained inside a single cryostat. During the design short circuit fault, the temperature of the former and HTS conductor layer of each phase increases to 93 K. A single cable core was selected for the analysis as the

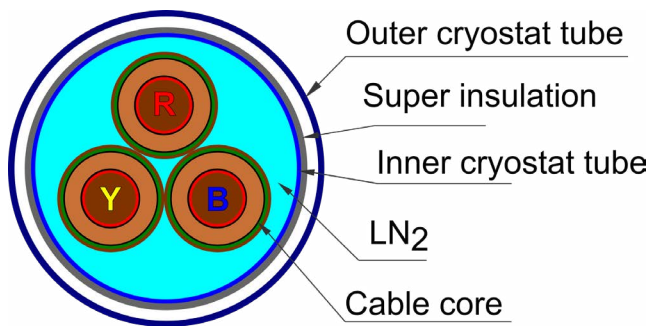


**Figure 4.** Cross section of a 3-in-One (Triad) type CD HTS cable

**Table 3.** Specifications of Albany, NY HTS Cable Project<sup>6</sup>

Item	Specifications
Cable type	AC, 3 phase, CD, Triad
Voltage, Current	34.5 kV, 800 A <sub>rms</sub>
Operating temperature	73 K
Former	Cu stranded wire
Electrical insulation	PPLP <sup>TM</sup> impregnated with LN <sub>2</sub> of 4.5 mm thickness
AC withstand voltage test	69 kV for 10 minutes
Fault current (Short circuit)	23 kA at 38 cycles for design
Temperature rise of HTS conductor	20 K

structural and operational characteristics of all the phases are similar.

## 2.2 Assumptions

Following are the assumptions used for the numerical analysis.

1. The former is considered as a solid cylinder.
2. The initial temperature distribution over each part of the domain was considered uniform.
3. The Joule heating at the former during the quench was considered to be adiabatic.
4. After the adiabatic heat generation, the heat transferred from the former is convected away uniformly from the outer surface of the cable core.
5. Since the study compares the thermal performance of two models, the common components with similar thermal characteristics can be neglected. They include the butt gaps, protective sheath of cable core, shield layer, copper stabilizer and semiconductor layers.
6. The thermal contact resistances between each cable layers and within the layers of dielectric were not considered.

## 3. Finite Element Analysis

The assumptions listed in section 2.2 were used to create computational domains for thermal and electrostatic analyses. The details of the numerical models of the cable used in this study are given in the following subsections.

### 3.1 Thermal Analysis

The thermal performances of HTS cables are compared based on their recovery time. Hence, emphasis was given to the temporal evolution of the temperature profile inside the cable during analysis. Due to the presence of intermittent thermal windows, the temperature distribution varies in the longitudinal as well as in radial direction of the cable. Consequently, a specific length of the cable is considered for the analysis. Since the butt gaps in the composite dielectric are not considered for the thermal analysis, symmetry around the longitudinal axis exists. Thus, a simplified two-dimensional domain is used in the numerical analysis.

A 100 mm section of the cable was selected for the analysis. It was assumed that thermal windows of 10 mm width are separated by 90 mm so that the thermal

window occupies 10% volume of the dielectric layer of the cable. The details of the computational domain are given in Figure 5. A mesh refinement at the interface between PPLP™ and copper was ensured. Due to the adiabatic nature of heat generation, it was assumed that the temperature of the former reaches 93 K while the dielectric remains at 73 K after the fault. Temperature-dependent material property values in the range of 73 to 93 K were used. Heat is convected away from the outer surface at a rate of  $6000 \text{ W/m}^2\text{-K}^{23}$ . A geometrically similar computational domain without the thermal window was used to simulate the conventional HTS cable. In both cases, the Static thermal module of ANSYS Workbench was used to define the initial condition and the results were transferred to the Transient thermal module for further analysis.

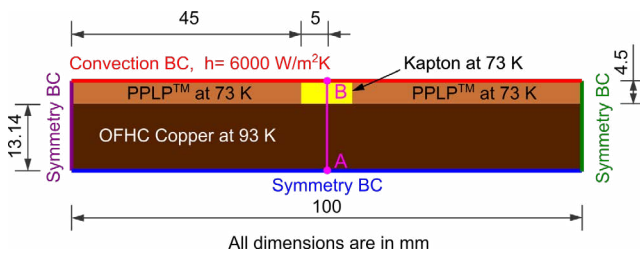


**Figure 5.** Computational domain for thermal analysis

### 3.2 Electrostatic Analysis

The objective of the analysis is to verify the electrical insulation characteristics of the dielectric layer by comparing the electric field distribution at the butt gaps and the thermal windows. Hence, the computational domain was selected such that it contains both composite insulation with butt gaps and thermal window as shown in Figure 6. It was assumed that the dielectric layer is composed of PPLP™ tapes of 25 mm width and  $250 \mu\text{m}$  thickness. Besides, they are wrapped over the former using the gap winding method with 26 mm pitch and 30% overlap. Hence, the dimensions and the distribution of the butt gaps were obtained which are given in the detailed view of Figure 6. The material properties are defined at the operating temperature of the cable. Following the AEIC code for 35 kV class cables, the cable had undergone an AC voltage withstand test<sup>6,21</sup>. Hence, a voltage of 69 kV was given at the bottom boundary of the computational domain keeping the top boundary at 0 kV. The Electrostatic module of ANSYS Maxwell was used to numerically solve the model.

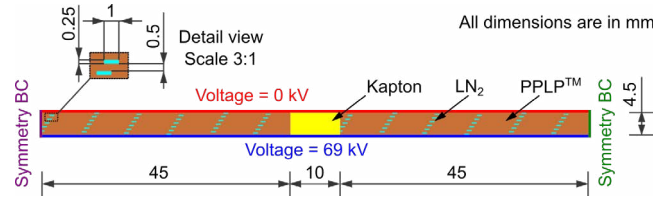


**Figure 6.** Computational domain for electrostatic analysis

## 4. Results and Discussion

Based on the above simulations, the outcomes are classified into thermal and electrostatic analysis results which are presented in the following subsections.

### 4.1 Thermal Analysis

Figure 7 shows the spatial distribution of temperature inside the computational domain at different instants of time for two dielectric designs. The temperature is plotted over path A-B as shown in Figure 5. Similar temperature profiles can be seen at time,  $t=0$  as the initial conditions are the same for both cases. However, a clear distinction between the temperatures at every node in the domain is visible in the following time steps. The temporal evolution of the maximum temperature at the cable core is plotted in Figure 8 for two dielectric configurations. It can be found that the dielectric layer having thermal windows requires less time to reach the same temperature as that of the dielectric layer consists only of PPLP™. For the considered 10% volume fraction of Kapton in the dielectric layer, an approximate reduction of 25% in the recovery interval is achieved. This corresponds to the enhanced heat transfer between the cable former and the  $\text{LN}_2$  in the annular flow passage.

### 4.2 Electrostatic Analysis

The electric field distribution inside the composite dielectric layer with thermal windows is shown in Figure 9. A horizontal path PQ is selected over the first half of the domain so that it passes through various points in the dielectric layer including butt gaps, dielectric material and thermal window. Electric field strengths at these locations are represented by the points A, B, C, D, E, F, G and H. Since the butt gaps are filled with  $\text{LN}_2$  having the lowest value of relative permittivity, higher values of the electric field can be found in these regions as depicted by the spikes A and D. Butt gaps are surrounded by low electric field regions which are represented by the troughs B, C,

E and G. Point H is located inside thermal window made of Kapton while F is at the dielectric made of PPLP™. It can be found that the electric field strengths at G and H are approximately equal since their relative permittivity values differ only by 12 %. Besides, the thermal window does not cause any electric stress in comparison with the composite dielectric where the maximum electric field is contained inside the butt gaps. Hence, it can be stated that

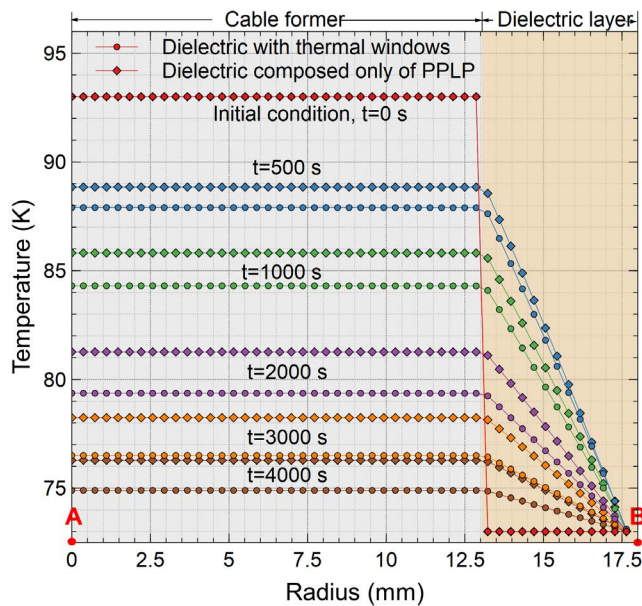


Figure 7. Spatial distribution of temperature in the radial direction at various instants of time.

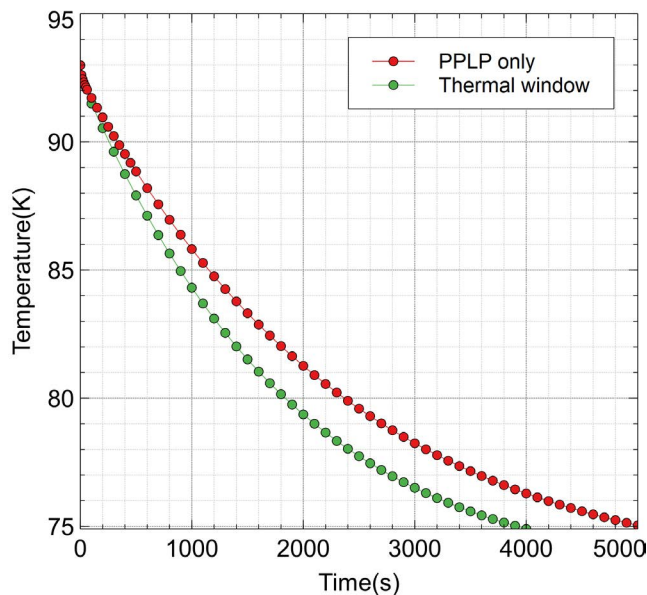


Figure 8. Temporal evolution of the maximum temperature inside the cable.

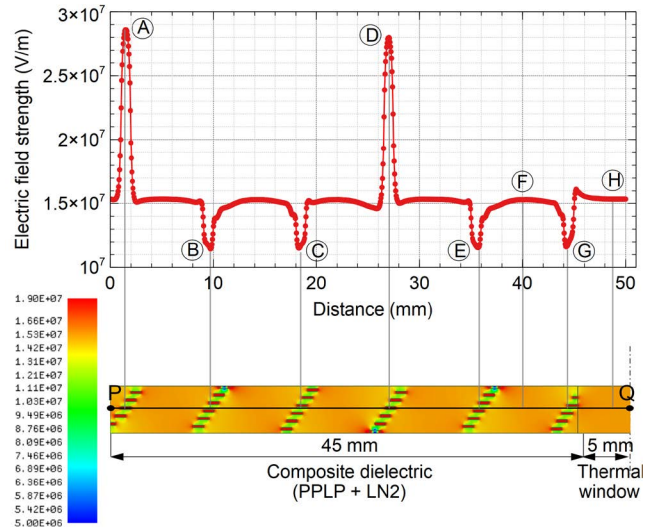


Figure 9. Electric field distribution inside the first half of the computational domain.

the electrical insulation limit of the presented dielectric layer design is governed only by the partial discharge inception voltage of the composite dielectric layer.

## 5. Conclusions

The present commercial design of CD HTS cables suffers from the long recovery interval after a quench which limits their commercial application. An innovative dielectric design for CD HTS cables using thermal windows was analyzed using FEA. Recovery intervals of the new and conventional HTS cable dielectric designs were compared. Furthermore, the effect of thermal windows on the electrical insulation characteristics was also studied. It was found that the introduction of thermal windows can reduce the thermal recovery interval of CD HTS cables without any deterioration in the cable insulation level. However, experimental investigations are required to verify the obtained results.

## 6. References

1. Hu N, *et al.* Fault current analysis in a tri-axial HTS cable. IEEE Transactions on applied superconductivity. 2010; 20(3):1288–91. <https://doi.org/10.1109/TASC.2010.2042941>
2. Sato Y, Agatsuma K, Wang X, Ishiyama A. Temperature and pressure simulation of a high-temperature superconducting cable cooled by subcooled LN<sub>2</sub> with fault current. IEEE

- Transactions on Applied Superconductivity. 2014; 25(3):1–5. <https://doi.org/10.1109/TASC.2014.2387119>
3. Kim S, *et al.* Investigation on the stability of HTS power cable under fault current considering stabilizer. IEEE Transactions on Applied Superconductivity. 2007; 17(2):1676–9. <https://doi.org/10.1109/TASC.2007.899208>
  4. Study committee SC21 HV insulated cables. High Temperature Superconducting Cable System. Italy : Cigré; 2003.
  5. Tuncer E, Zuev YL, Sauers I, James DR, Ellis AR. Electrical properties of semiconducting tapes used in HTS power cables. IEEE transactions on applied superconductivity. 2007; 17(2):1497–500. <https://doi.org/10.1109/TASC.2007.899961>
  6. Masuda T, *et al.* Design and experimental results for Albany HTS cable. IEEE Transactions on Applied Superconductivity. 2005; 15(2):1806–9. <https://doi.org/10.1109/TASC.2005.849296>
  7. Gawith JDD, *et al.* An HTS power switch using YBCO thin film controlled by AC magnetic field. Superconductor Science and Technology. 2019; 32(9). <https://doi.org/10.1088/1361-6668/ab2d61>
  8. Hu, N., *et al.* Transient thermal analysis of a tri-axial HTS cable on fault current condition. Physica C: Superconductivity. 2013; 494:276–9. <https://doi.org/10.1016/j.physc.2013.05.012>
  9. Hu N, Toda M, Watanabe T, Tsuda M, Hamajima T. Recovery time analysis in a tri-axial HTS cable after an over-current fault. Physica C: Superconductivity and its applications. 2011; 471(21–22):1295–9. <https://doi.org/10.1016/j.physc.2011.05.181>
  10. de Sousa, WTB, Kottonau D, Noe M. Transient simulation and recovery time of a three-phase concentric HTS cable. IEEE Transactions on Applied Superconductivity. 2019; 29(5):1–5. <https://doi.org/10.1109/TASC.2019.2900937>
  11. Li, Ming Z, *et al.* Temperature and current distribution of high temperature superconducting cable itself under large fault current. 2015 IEEE International Conference on Applied Superconductivity and Electromagnetic Devices (ASEMD). IEEE; 2015. <https://doi.org/10.1109/ASEMD.2015.7453510>
  12. Takahashi T, *et al.* Dielectric properties of 500 m long HTS power cable. IEEE Transactions on Applied Superconductivity. 2005; 15(2):1767–70. <https://doi.org/10.1109/TASC.2005.849281>
  13. Choi YS, Kim DL, Shin DW, Hwang SD. Thermal property of insulation material for HTS power cable. AIP Conference Proceedings. 2012; 1434(1):1305–12. <https://doi.org/10.1063/1.4707055>. PMID:22042559
  14. Choi YS, Kim DL. Thermal property measurement of insulating material used in HTS power device. Cryogenics. 2012; 52(10):465–70. <https://doi.org/10.1016/j.cryogenics.2012.05.003>
  15. Manfreda G. Review of ROXIE’s material properties database for quench simulation. TE Technology Department Internal Note; 2011. p. 35.
  16. Iwasa, Yukikazu. Case studies in superconducting magnets: design and operational issues. Springer Science & Business Media; 2009.
  17. Tuncer, Enis, *et al.* Electrical properties of commercial sheet insulation materials for cryogenic applications. 2008 Annual Report Conference on Electrical Insulation and Dielectric Phenomena; 2008. <https://doi.org/10.1109/CEIDP.2008.4772931>
  18. Jensen, JE, Stewart RG, Tuttle WA, Brechna H. Brookhaven national laboratory selected cryogenic data notebook: Sections I-IX (Vol. 1). Brookhaven National Laboratory; 1980.
  19. Tuncer E, Polizos G, Sauers I, James DR, Ellis AR, Messman JM, Aytuğ T. Polyamide 66 as a cryogenic dielectric. Cryogenics. 2009; 49(9):463–8. <https://doi.org/10.1016/j.cryogenics.2009.06.008>
  20. Schmidt F, Allais A. Superconducting cables for power transmission applications-a review. In Paper submitted to Proceedings of this workshop; 2004.
  21. Yumura H, *et al.* 30 m YBCO cable for the Albany HTS cable project. Journal of Physics: Conference Series. 2008; 97(1). <https://doi.org/10.1088/1742-6596/97/1/012076>
  22. Yumura H, *et al.* Phase II of the Albany HTS cable project. IEEE Transactions on Applied Superconductivity. 2009; 19(3):1698–701. <https://doi.org/10.1109/TASC.2009.2017865>
  23. Del-Rosario-Calaf G, Lloberas-Valls J, Sumper A, Granados X, Villafafila-Robles R. Modeling of second generation HTS cables for grid fault analysis applied to power system simulation. IEEE Transactions on Applied Superconductivity. 2012; 23(3):5401204-<https://doi.org/10.1109/TASC.2012.2236673>